Real-Time measurement of the plasma electron density at ISTTOK and study of the ISTTOK hydrogen injection system *

Tiago Guerra Marques (tmarques@ipfn.ist.utl.pt)
Associação Euratom/IST Instituto de Plasmas e Fusão Nuclear, Instituto Superior Técnico 1049-001 Lisboa, Portugal

This paper presents the system developed for the real-time calculation of the plasma electron density at the ISTTOK tokamak. This variable is a fundamental parameter in a fusion plasma and its knowledge is essential for the real-time control of the plasma. The microwave interferometer (100 GHz) was chosen as the diagnostic used due to its simplicity and quality of results.

A low cost, embedded system was developed for the real-time calculation of the plasma density, which consists on a board with analog inputs where the interferometers outputs are connected, responsible for the signal conditioning, followed by another board with a dsPIC that digitizes, calculates, detects a discharge at the ISTTOK and sends the results by serial communication through an UART module.

The maximum frequency for the calculation of the electron density is 98.30 ksps, though the calculation itself only takes 3.8 μs. The system produced results with great quality, very close to those of the offline calculation, in an extremely reliable way.

A possible application of the system developed is the real-time control of the hydrogen injection by puffing, essential in long discharges (longer than 250 ms), by sending a PWM to the piezoelectric valve. However, a study of the actual system revealed that this must be improved, since too much hydrogen is being injected which could be harmful to the plasma.

Keywords: Tokamak, Data acquisition, Real-time diagnostics, Digital signal processor, Interferometry, Plasma fuelling

1. INTRODUCTION

In nuclear fusion a real-time control of the plasma is essential not only for security issues but also to help maintain the ideal conditions essential for the plasma stability.

The electron density is a fundamental parameter of the plasma and must be measured during discharges. At the ISTTOK tokamak (a circular cross section, iron core transformer, limiter tokamak) the microwave interferometer allows the offline determination for the plasma electron density during a discharge. However, if a real-time control of the plasma that involves electron density knowledge is to be implemented, a real-time diagnostic of this variable must first be developed.

Table I: ISTTOK main parameters (*Data taken from [8]*).

Parameter	Value
Major radius	460 mm
Copper shell radius	105 mm
Minor radius	85 mm
Aspect ratio	5.75
Plasma volume	0.06 m^3
Magnetic toroidal field	0.3 - 0.6 T
Plasma current	3 - 6 kA
Electron density	4 - 10 $\times$ 10^{18} m^{-3}
Electron temperature	150 - 230 eV
Cycle duration	25 ms

Operation of the ISTTOK tokamak in a multicycle alternating square wave plasma current regime (AC) [9] has permitted to achieve 250 ms discharges [10] (figure 1). However, in the final moments of the discharge the plasma is in a much worse condition than in the beginning. This is probably due to particle losses and changes in recycling on the limiter and walls. Therefore, in order to maintain the plasma stability in long discharges, more hydrogen needs to be injected at certain instants to counterbalance these losses. This could be

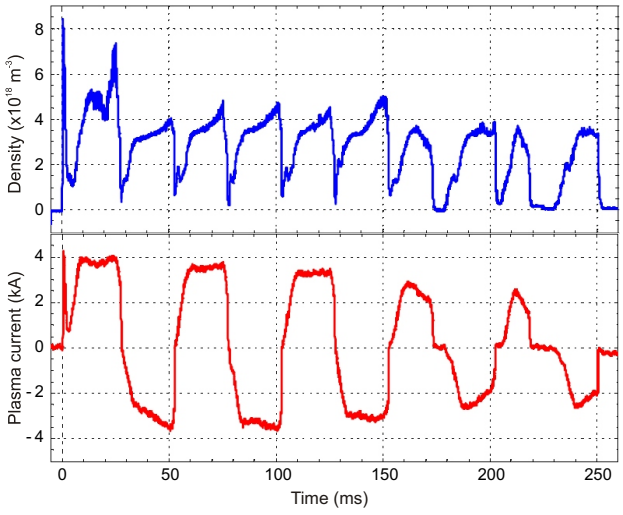

Figure 1: Electron density and plasma current for a long discharge (250 ms). In the last four cycles the plasma is less stable.

*Extended Abstract.

done by a real-time control of the puffing system. Real-time plasma electron density is one fundamental control variable for this process loop.

This paper presents the system developed for the real-time calculation of the electron density, using data from a single-channel microwave interferometer ($\lambda_0 = 3$ mm), probing the plasma on its center. While this type of calculation has been done for many years in several systems [16] [17], most are analogic. Some purely digital systems are starting to appear in newer devices due to their low cost and reliability [18].

Ours consists on a low-cost approach using a dsPIC (digital signal Programmable Intelligent Computer) embedded system, allowing phase measurements with a 62 mrad resolution at 98.30 ksps. This kind of precision is extremely important in our system since in each discharge very few interference fringes occur (typically two). The calculation itself only takes 3.8 μs. The system produced results with great quality, very close to those of the offline calculation, in an extremely reliable way.

For a better understanding of the system projected, a brief introduction to interferometry theory is presented on section 2. In section 3 the various steps of the system development are explained and the results obtained for several plasma discharges at the ISTTOK are presented in section 4. Section 5 contains the study of the hydrogen injection by puffing performed at the ISTTOK, fundamental for an understanding of how the localized injection of hydrogen affects the plasma. Finally, in 6 the conclusions of this project are summarized.

2. TOPICS ON INTERFEROMETRY

A. Physical Principal

Interferometry consists on the technique of overlapping two or more waves, detecting this way their differences in phase. Tipically, in an interferometer, a wave is divided in two or more coeherent parts that propagate through different paths. After a while the waves are combined in such a way that they interfer with each other. So, an interferometer is a measurement instrument sensible to a medium that alters the phase of a wave such as the path length or the refractive index. This way, for determining the medium characteristic one wishes to study, it is only needed to measure the difference in phase that the electromagnetic waves undergo when propagating in a sample of the material.

B. Interferometry as an Electron Density Diagnostic

Interferometry of electromagnetic waves was one of the first experimental diagnostics being used for measuring the plasma electron density due to its high reliability. Its principle relies on the combination of two waves and on the dielectrical properties of the plasma. If one of the waves travelled across a plasma column, its phase carries information about the plasma's refractive index which, for a linearly polarized wave with electrical field parallel to the toroidal magnetic field, is related to the plasma electron density. The phase difference introduced by the plasma relatively to the same path on vacuum is given by

$$\Delta\phi_p(t) = \frac{2\pi}{\lambda_0}\int_l \left\{1 - \left[1 - \frac{n_e(z)}{n_c}\right]^{\frac{1}{2}}\right\} dz, \qquad (1)$$

where $n_e(z)$ is the electron density along the path l on the plasma and n_c is the critical density, defined as the density above which the electromagnetic wave with a certain frequency (ω) is not able to propagate. This parameter can be obtained by replacing the plasma frequency (ω_{pe}) by the wave frequency (ω) and solving to find the electron density

$$n_c = \frac{\epsilon_0 m_e \omega^2}{e^2}\,. \qquad (2)$$

If the plasma density is much lower than the critical density, to the first order n_e/n_c, which corresponds to probing the plasma with a frequency much higher than the plasma cut-off frequency, one can solve equation 1 for the average electron density integrated along the path

$$\bar{n}_e(t) = \frac{\lambda_0 n_c}{\pi l}\Delta\phi_p(t)\,. \qquad (3)$$

C. ISTTOK Microwave Interferometer

The ISTTOK interferometer was projected as single-channel microwave heterodyne system with quadrature detection for an absolute phase determination. The plasma probing frequency is 100 GHz ($\lambda_0 = 3$ mm) which corresponds to a critical density of 1.24×10^{20} m^{-3}. The approximation stated on the previous section can, then, be used because the maximum possible electron density is $n_e(0) = 3.75 \times 10^{19}$ m^{-3}. Since the plasma is probed at the central chord, the length of the path l is twice the plasma minor radius and equation 3 becomes

$$\overline{n_e}(t) \approx 6.964 \times 10^{17}\Delta\phi_p(t)\,. \qquad (4)$$

3. CONCEPTION OF THE REAL-TIME SYSTEM

A. Phase Calculation

An interferometer with quadrature detection, has two output signals.

$$V_{1out} = V_{1DC} + K_1\cos(\Delta\phi_p(t)) \qquad (5)$$

$$V_{2out} = V_{2DC} + K_2\sin(\Delta\phi_p(t)) \qquad (6)$$

Since what is required is the phase shift $\Delta\phi_p(t)$, it can be easily obtained using the arctan function in the four quadrants after eliminating the offsets and taking into account the gains of each channel.

$$\Delta\phi_p(t) = \arctan_{4Q}\left(\frac{K_1\left(V_{2out} - V_{2DC}\right)}{K_2\left(V_{1out} - V_{1DC}\right)}\right) \quad (7)$$

Equation 7 is the one that should be used for calculating the phase shift introduced by the plasma when using the quadrature signals from the interferometer. However, this is not enough since it is also necessary to count the interference fringes (complete turns of the trigonometric circle). This is done thanks to the *unwrap* algorithm which consists on comparing two successive phases ($\Delta\phi_{p_n}$ and $\Delta\phi_{p_{n+1}}$). If $\Delta\phi_{p_{n+1}} - \Delta\phi_{p_n} < -\pi$, a positive complete turn has been achieved and 2π is added to the phase shift. To detect a negative turn in the trigonometric circle the difference between both values should be superior to π and -2π will be added to the phase shift.

B. Interferometer Signal Analysis

1. Signals Offsets and Gains

It is essential to study the interferometer quadrature outputs before developing the real-time system. Correcting the offsets and gains of the interferometer outputs is essential for a correct phase shift calculation. Since during one discharge at least one interference fringe is achieved, the maximum and minimum sampled correspond to the absolute maximum and minimum of the signals. Therefore, both the offset and the amplitude can be calculated offline using

$$offset_{signal} = \frac{V_{signal_{max}} + V_{signal_{min}}}{2} \quad (8)$$

$$amp_{signal} = \frac{V_{signal_{max}} - V_{signal_{min}}}{2} \quad (9)$$

Regarding the offsets, not only these were different in both signals, but also they were not constant in time. In successive discharges this effect was not significant, resulting in just small fluctuations. However, during days of operation of the ISTTOK the offsets oscillated considerably. As for the gains of the signals, it was also verified that they varied slightly from discharge to discharge but now both signals presented similar amplitudes (with differences around 2%). This way, the gains correction is not mandatory since the signals are divided during the phase calculation and the gains cancel each other.

2. Sampling Requirements

Studying the Fourier transforms of the signals is very important in determining the minimum sampling frequency to avoid alliasing. Both interferometer signals pass through a second order low-pass filter, which cutoff frequency can be chosen from three values: 8, 16 and 32 kHz.

Alliasing is avoided if for frequencies higher than the Nyquist (half the sampling frequency), the signal is sufficiently reduced, below the ADC resolution (out of its dynamic range). The requirements regarding the sampling rates for an ADC with a certain resolution to be used are presented in table II.

Table II: Sampling requirements to achieve a certain ADC resolution

Resolution	$f_{cutoff} = 8$ **kHz**		$f_{cutoff} = 16$ **kHz**	
	$f_{Nyquist}$ **(kHz)**	$f_{sampling}$ **(ksps)**	$f_{Nyquist}$ **(kHz)**	$f_{sampling}$ **(ksps)**
6-bits	8	16	8	16
8-bits	12	24	20	40
10-bits	22	44	44	88
12-bits	-	-	-	-

The values for the 32 kHz filter cutoff frequency are not present on the table since in this case a 10-bits ADC could not be used for a sampling frequency below 100 ksps. The same was verified for a 12-bits ADC in all the three cutoff frequencies.

This way, the choice of the sampling rate will have to take into account the resolution of the ADC and should dictate the filter cutoff frequency. Considering the 6-bits ADC as the minimum resolution to be used, the sampling should be made at least at 16 ksps.

3. Fringe Counting

The sampling frequency must also take into account the interference fringe counting. If the sampling is performed at a very low rate, it is possible that some fringes are missed during the *unwrap* function and the phase shift obtained presents an error multiple of 2π (which corresponds to an electron density of 4.38×10^{18} m^{-3}). This error is of the same order of magnitude of the values of the electron density registered at the ISTTOK and, therefore, missing just one fringe produces invalid results. So, this question is of extreme importance since it must be guaranteed that all fringes are counted.

To study the importance of the sampling rate in the fringe counting the signals stored in the data base were decimated and used for the electron density calculation. As an example, a signal originally sampled at 100 ksps with a decimation factor of 10 corresponds to an acquisition of 10 ksps. This way, several stored signals (sampled at 200 ksps) were decimated and analyzed and the lowest maximum tolerable decimation factor observed was 9.

This means that for a sampling frequency of $^{200}/_{9} = 22.22$ ksps, in principle, no mistakes in the fringe counting will be made. Considering that in the limit, at least

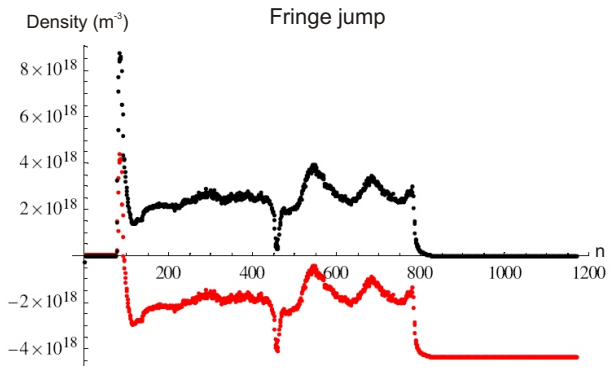

Figure 2: Fringe jump at discharge #18181 with a decimation factor of 14. The black curve represents the correct plasma electron density and the red curve the results obtained after the decimation.

two points need to be sampled in each trigonometric circle for the fringes to be counted correctly, this frequency allows electron density variations detections up to 4.89×10^{22} m^{-3}s^{-1}.

To ilustrate this issue, figure 2 shows the graphics of the density obtained after the decimation (red) and the correct result (black) with a decimation factor of 14 for discharge #18181. It can be easily observed that during the peak in the beginning of the discharge (important for the ignition of the plasma) the electron density rises so fast that an interference fringe is lost during the *unwrap* function with the decimated signals. This results in a phase shift decrease of 2π relatively to the real value. After the fringe jump, the plasma electron density is 4.38×10^{18} m^3 below what it was supposed to be.

C. Choice of Hardware

1. Microprocessor

The project specifications demanded two analog channels for data acquisition, sampling frequency sufficiently high to count the fringes and avoid alliasing, processor speed relatively high for the phase determination and a communication module for sending the results at 1 kHz. The microcontroller chosen was the dsPIC30F4013 [22] [23] due to its easiness of use, versatility and low-cost.

In terms of speed, the microcontroller uses an external crystal oscillator and a PLL (Phase Locked Loop) to obtain a clock frequency of 117.9648 MHz (f_{OSC}). Since each instruction needs 4 clock cycles, the instruction frequency (f_{CY}) is 29.4912 MHz.

The microcontroller possesses an UART (Universal Asynchronous Receiver/Transmitter) module responsible for asynchronous serial communication in full-duplex.

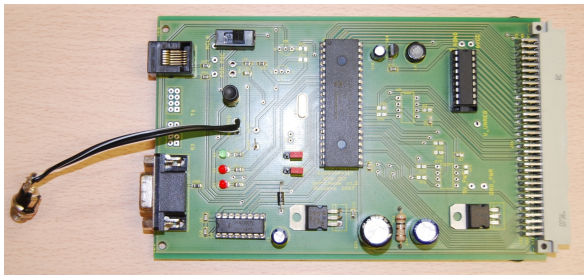

Figure 3: Microprocessor board for the power supply and I/O's ports.

This communication can be made at the standard baud rates 9600, 19200, 38400, 115200 and 460800 by RS232 and also 921600 and 1843200 by optic fibre with no error. Due to the low transmission rates necessary for this project, the communication was established by RS232 connecting the D9 port on the board with the serial port of a computer.

Finally, the microcontroller has an ADC module with one 12-bits ADC, with a maximum sampling rate of 200 ksps, 16 analog inputs and a Sample/Hold circuit. The fact that only one ADC is available can be troublesome since two signals need to be sampled simultanously. This can be partly solved by sampling two channels in a multiplexed way and synchronizing the measurements afterwards. For this project the sampling rate must be divided by two, because two channels are being sampled. This leads to a maximum sampling rate of 100 ksps which does not allow the 12-bit resolution.

2. Signal Conditioning Board

The analog input range of the ADC is [0; 5] V which is incompatible with the interferometer outputs ([-5; 5] V). This way, a small signal conditioning circuit needs to be projected. This can be easily achieved by first reducing the voltage range into half (an amplification of 1/2) and then creating an offset of 2.5 V. A simple summing amplifier was projected to perform this, consisting on 4 resistors, 1 capacitor and one low-power operational-amplifier. The circuit transforms the [-5; 5] V from the interferometer outputs to [0; 4.762] V compatible with the ADC input. Since there are two signals to be sampled, two duplicate circuits were implemented on the same signal conditioning board that connects to the microprocessor board.

D. Microprocessor Programming

1. Overview

The central part of this project is the microprocessor programming. It is the microcontroller that is going to

be responsible for the interferometer signals acquisition, the phase shift calculation and the communication with an external device to send the results.

The microprocessor was programmed in C due to its simplicity. Although the C allows the use of many functions to simplify the dsPIC configuration, our approach was closer to assembly by writing directly into the microprocessor registers to maximize the performance of the program, which is essential in a real-time application.

2. A/D Module

The configuration of the A/D module of the microcontroller is extremely important for this project since it involves the acquisition of two analog signals.

The time it takes to perform an acquisition is given by the sum of the sampling time (ST) with the conversion time. The conversion time is 14 ADC clock cycles (T_{AD}) - 12 cycles for each bit and one more before and after the acquisition. The sampling time can be defined by the programmer in multiples of T_{AD} with 1 T_{AD} being the minimum. Therefore, in order to specify the sampling frequency, it is just necessary to configure the number of T_{AD} for the sampling time and the duration of the T_{AD} itself.

To overcome the impossibility of sampling the two interferometer outputs at the same time, the channels were sampled alternately and then a linear interpolation of one of the channels (cos) was performed. This method, however, introduces an error in one of the signals that increases with the acquisition time.

This way, the configuration of the A/D Module consisted on choosing the sampling and the conversion time and selecting the automatic sample and convert option while scanning both channels. Each time a pair of values is obtained their value is stored and data is processed while a new sampling is taking place. The maximum sampling frequency for this method is 98.30 ksps.

3. Phase Shift Calculation

Following the acquisition of the interferometer outputs is the central part of the program that consists on the phase shift calculation. This calculation consists on a table of the arctan function in the first quadrant, with the absolute value of the integer ratio $^{\sin}/_{\cos}$ pointing into it. The other quadrants ($\pi/2$ to 2π) are found by signal inspection.

To improve the resolution of this method instead of using the ratio $^{\sin}/_{\cos}$ as a pointer to the table, $^{16\sin}/_{\cos}$ (the multiplication of sin by 16 is performed before the division) is used. Since the adquired signals only possess 12 bits, a multiplication by 16 can be easily made by performing 4 left shifts without any danger of overflow. This way when the pointer is 1, pointing to the first table position, it follows that $^{\sin}/_{\cos} = {}^{1}/_{16}$ which arctan is 62.42 mrad (the resolution of this method). Since the microcontroller has a data memory of 1 k words, a table with 953 positions was constructed leaving space for other program variables. The table last entry is 1.553 rad, which is only 17.80 mrad away from the maximum value.

The *unwrap* function was implemented exactly as it was previously described.

4. UART Module

The UART configuration required is quite simple, since only a result of the phase shift needs to be sent after a certain number of calculations. The data was sent in the 8-bit format with no parity and just one stop bit. The data reception was made in a computer via serial port with an altered version of the hyperterminal that allows the values visualization in decimal instead of in the ASCI code as usually happens.

Since the phase shift is coded as a 16-bits integer, every time that a result needs to be sent, it is first necessary to split it into two 8-bits words. As the UART module has a 4-words deep FIFO buffer for data transmitting, this can be easily done using two masks.

Each time the phase shift is calculated the number of the acquisition is divided by an integer (*divisor*) set by the programmer. When the remainder of the division is 0 (% operator in C), the result is transmitted. For example, if the the sampling rate is 50 ksps and the transimission frequency to be implemented is 2 kHz, the value of this *divisor* is 25. This way two phase shift results will be transmitted each ms.

Although the main goal regarding results transmission was one result each ms, higher rates can be used without affecting the overall performance of the system.

Table III: Maximum number of outputs in one ms

Baud Rate	**Maximum transmission frequency (kHz)**	**Transmissions per ms**
19200	1.07	1
38400	2.13	2
115200	6.40	6
460800	25.60	25
921600	51.20	51
1843200	102.40	102

5. Final Program

There are still two details regarding the offsets of the signals and the phase shift left to be explained.

First, not correcting the signals offsets would produce incorrect results since they do not cancel on the ratio

$^{sin}/_{cos}$. In an offline phase calculation the offsets are calculated with the knowledge of all the points in the discharge. However, this is not possible in a real-time calculation and a different approach must be considered. As it was previously referred the offsets do not vary considerably when considering two successive discharges and, as a first approximation, they can be considered constant. This way, during a discharge the maximum and minimum of both signals are stored and after the end of the discharge the offset is calculated as the average. This value will then be used in the next discharge by subtracting it to the sampled measurements of the signals.

As for the calculation of the phase shift offset, a similar approach will be used. When switching on the microcontroller or at the end of a discharge, an eight values average of the phase shift is performed in order to filter high frequency noise. These values correspond to the phase shift when no discharge is taking place which is exactly the phase offset. During a discharge this value will be subtracted to all calculated phase shifts.

This average is also very useful to perform the trigger of a discharge. After its determination still before a discharge, each time the phase is calculated it is compared to the phase shift offset. If their difference is higher than $\pi/2$, then a discharge has taken place and the program changes from *iddle* to *shot* state and starts transmitting the phase result at the programmed frequency. The value of $\pi/2$ was used as the trigger level since this was sufficiently high to do not detect the electrical noise and since it corresponds to a quarter of an interference fringe, it will not miss a fringe in the beginning of the discharge.

The program can be configured in several ways, allowing the choice of the sampling rate and the way this is done (more time in the sampling or in the conversion), the data transmission frequency and the duration of the discharge.

Finally, table IV shows the processing times of several sequences of code.

Table IV: Processing times of the several tasks executed during the program

Task	**Processing time (μs)**
Acquisitions storage, sin shift and cos interpolation	0.4
Extreme verification for both signals	0.6
Phase calculation	1.7
Unwrap	0.4
Result output	0.7
Total	**3.8**

The total, represents all the tasks that need to be executed in an acquisition cycle in the worst case scenario.

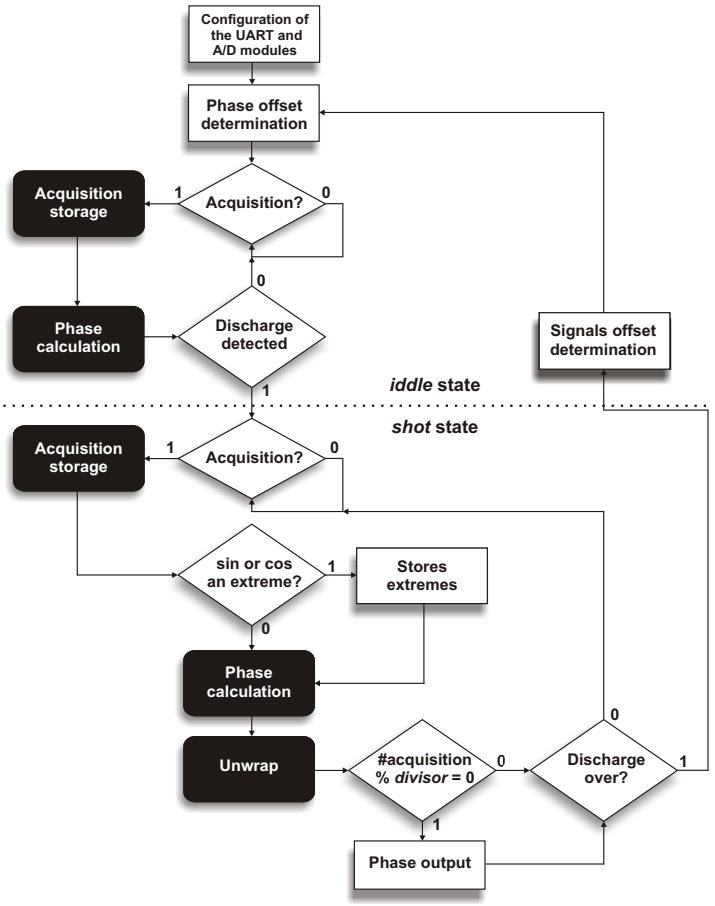

Figure 4: Program flowchart. The program begins by configuring the UART and A/D modules. Then the phase offset is calculated as the 8-points average. Each time an acquisition is performed the phase is calculated and compared with the offset. If a discharge is detected, then the program changes to *shot* state. There, with each acquisition, besides the phase calculation, there is a test to see if the measurements correspond to extremes and the *unwrap* algorithm is executed. At the programmed frequency the result is transmitted and this cycle is repeated until the discharge is over. When this happens the signals offset are calculated and the program returns to the beginning.

E. System Overview

The system developed consisted on a low-cost purely digital approach to the real-time calculation of the plasma electron density. Its main features are the following:

- Several possible configurations regarding sampling and data transmission rates;
- Sampling rate up to 98.3 ksps;
- Calculation cycle of 3.8 μs (263.2 kHz);
- Algorithm resolution of 62 mrad (1% of an interference fringe);

- Automatic correction of the signals and electron density offsets;
- CPU cycle free time of 6.4 μs when using the maximum sampling rate;
- Maximum transmission frequency of 102.4 kHz (limited by the sampling frequency);
- Analog input range of [-5; 5] V;
- Phase shift range of [-5.22 $\times 2\pi$; 5.22 $\times$ 2π] rad;
- Maximum plasma electron density of 2.29 $\times$ 10^{19} m^{-3};
- Detects electron density variations up to 2.16 $\times$ 10^{23} m^{-3}s^{-1};
- Low latency (3.8 μs plus transmission time);
- High system versatility.

Although the system was concepted for the ISTTOK tokamak, it can be easily adapted to other devices by some reconfigurations and a different signal conditioning.

4. TESTS AND EXPERIMENTAL RESULTS

To test the real-time system several similar discharges with two AC cycles were performed at the ISTTOK. The low pass filter cutoff frequency was set at 8 kHz so that a 10-bit resolution of the ADC was achieved on most of the discharges (sampling rate must be at least 44 ksps). Some different configurations of the real-time system were studied to see how these affected the results produced.

The real-time results were compared with the offline calculation. This last was made with the results stored in the data base sampled at 100 ksps. To present both graphics overlapped (real-time and offline calculations) it was first necessary to synchronize them. The time between samples of the offline results is 10 μs while for the real-time calculation it is given by

$$tbs_{RT} = \frac{1}{f_T} = \frac{divider}{f_s} \qquad (10)$$

where tbs_{RT} is the time between samples of the real-time system, f_T is the transmission frequency and f_s is the sampling frequency.

A time shift must also be performed because while the samples acquired by the ISTTOK control and data acquisition system all start at 5 ms before the discharge, the results from the real-time system start at the first moments of the discharge (after the system automatic trigger).

The results are overall very good with a great concordance between the real-time calculation and the offline (figure 5 shows a typical discharge observed.). In spite of all the real-time system limitations (no gain correction, virtual synchronization of both channels acquisitions, offset correction using the offsets of the previous discharge and a lower sampling rate), the system proved extremely reliable. All the discharges performed at the ISTTOK were detected and no false triggers occured. Also extremely important was the fact that in all the discharges, many more than the presented in this paper, no fringe was ever missed.

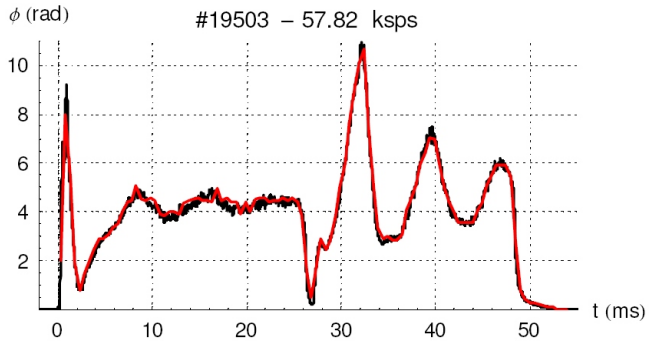

Figure 5: Discharge #19503 (T_{AD} = 508.6 ns and ST = 3 T_{AD}). Black curve represents the offline calculation while the red curve the real-time system (57.82 ksps).

Despite the good results, in some discharges it is clear that some significant differences in the curves exist. Figure 6 shows one of these cases. The configuration of this discharge corresponds to the maximum sampling rate allowed by the system. One could initially have thought that the quality of results improved with the increasing of the sampling rate due to the error commited by the linear interpolation of the cos channel (for the virtual synchronization). However, it was observed that the discharges where the real-time system behaved worsely were the ones with higher sampling rates. This is only notorious when the T_{AD} is near its minimum acceptable value (333 ns). This probably happens because the ADC is operating very closely to its limit which seems to affect severely the quality of the acquisitions.

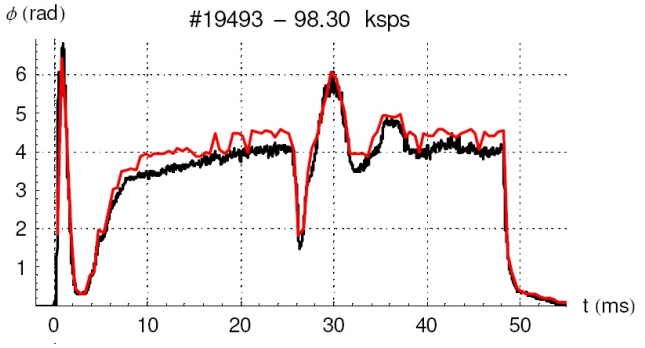

Figure 6: Discharge #19493 (T_{AD} = 339.1 ns and ST = 1 T_{AD}). Black curve represents the offline calculation while the red curve the real-time system.

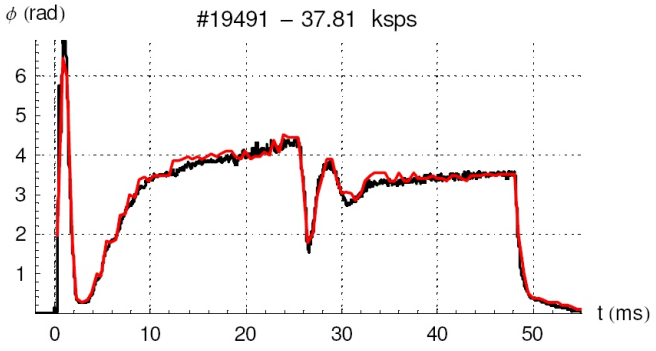

Figure 7: Discharge #19491 (T_{AD} = 339.1 ns and ST = 25 T_{AD}). Black curve represents the offline calculation while the red curve the real-time system (37.81 ksps).

On the other hand, decreasing the sampling rate too much (figure 7) also seems to affect the quality of the results, though not as significantly as in the other extreme. In the discharge shown the sampling rate is below the needed for a 10-bit resolution.

Finally, one other result was the importance of correcting the offsets of both interferometer outputs. Figure 8 shows a discharge with exactly the same configuration as the one in figure 5 but without offset correction. By observing the graphics it is notorious that correcting the offsets improved significantly the quality of the results.

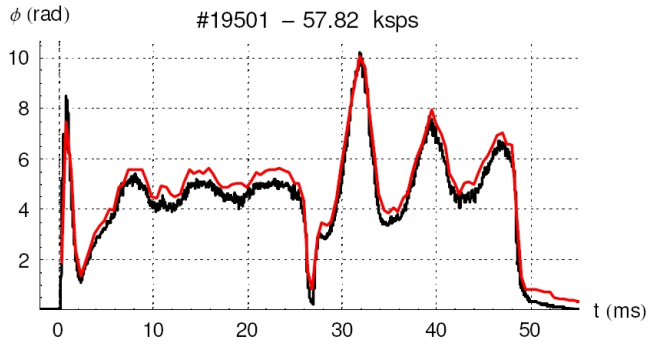

Figure 8: Discharge #19501 (T_{AD} = 508.6 ns and ST = 3 T_{AD}). Black curve represents the offline calculation while the red curve the real-time system (57.82 ksps). No signals offset correction.

5. STUDY OF THE PUFFING SYSTEM

As previously described, it is essential to fuel the tokamak plasma with particles during a long discharge to assure a minimum pressure that keeps the plasma stable (losses to pumps and walls/limiter). This is usually done by gas puffing at the plasma edge due to its high reliability and little hardware. The puffing at the ISTTOK is performed thanks to the MaxTeK MV-112 piezoelectric valve [28] (Q_{1atm} = 800 cm^3/min).

It is possible to estimate the throughput through the piezoelectric valve, responsible for the puffing, considering it linear with the inlet pressure:

$$Q_{600\ \mathrm{mbar}} = Q_{1atm}\frac{0.6\ \mathrm{bar}}{1\ \mathrm{atm}} = 7.9\ \mathrm{cm}^3/\mathrm{s} \qquad (11)$$

Considering 1 ms of puffing, a volume of 7.9x10^{-3} cm^3 is injected. This gas corresponds to 115 × 10^{15} H_2 molecules and would be responsible for a pressure of 5.2 × 10^{-5} mbar inside the ISTTOK vacuum chamber (V_{tok} = 90.8 dm^3) at 25 °C. This value is one third of the background pressure of a typical discharge (p_{tok} = 1.5 × 10^{-4} mbar).

The system experimental study consisted on performing a single pulse puffing on the first plateau during a four cycle AC discharge. This way it is possible to determine the effect of a localized hydrogen injection on the plasma. The puffing pulse was pre-programmed to start at 10 ms after the beginning of the discharge and several different durations were tested (1.5, 2, 2.5 and 3 ms and no puffing). It is useful to note that the valve is not open during the whole pre-programmed pulse since it needs to be taken into account the time it takes to open. Previous results indicated that the time the valve stays open is obtained by subtracting 800 μs to the duration of the pulse.

In the graphics (figure 9) it is possible to observe that while the 1.5 ms puffing practically does not affect the plasma, the 2 ms is responsible for a slight decrease in density and plasma current. As for the 2.5 and 3 ms puff-

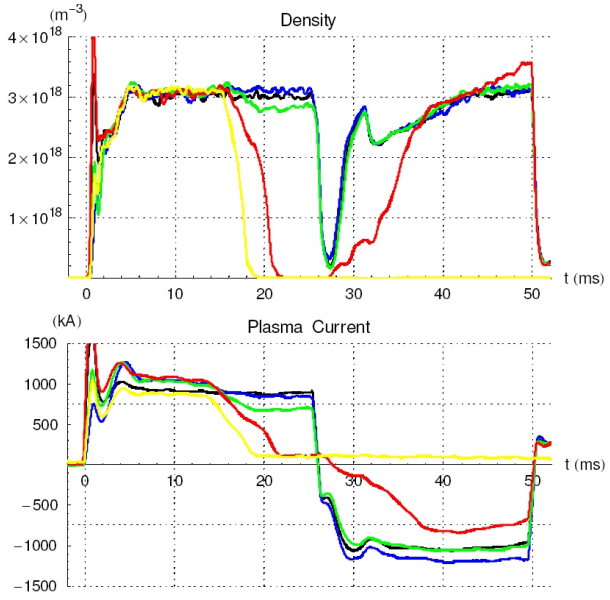

Figure 9: Density and Plasma Current for the first two cycles of the discharges with a single pulse puffing performed at 10 ms (black - no puffing; blue - 1.5 ms; green - 2 ms; red - 2.5 ms; yellow - 3 ms).

ing discharges, it is evident that the plasma extinguishes right on the first cycle. While on the 3 ms puffing discharge there is no more plasma until the end of the shot, on the 2.5 ms the plasma ignites right on the second cycle. Although the plasma is considerably weaker on this cycle, on the third and fourth cycle (not shown here) no differences between the different discharges were observed.

Another important observation to be referred is that the effects of the puffing are only visible around 4 ms after the start of the pulse. This delay is probably due to the signal transmission time, the time the valve takes to open and the propagation of the gas inside the tubes.

In theory, when injecting gas into the plasma, part of it should be ionized, increasing this way the electron density. The ionization of the gas cools the plasma at the first moments since it needs to transfer some of its energy which in turn lowers the plasma current. After a while, the plasma current should stabilize around a certain equilibrium.

The results obtained were significantly different from these views. The electron density, instead of increasing, decreases and eventually goes to 0 when the puffing is sufficiently long. This is thought to happen because the quantity of the hydrogen injected is too big for the plasma in the tokamak.

To estimate the quantity of injected gas in each discharge, the value of the quantity injected per ms by the piezoelectric valve was used ($\dot{n}_{\mathrm{H}_2} = 115 \times 10^{15}$ H_2 molecules) and the 800 μs delay in the opening of the valve was considered. Equation 12 shows how to calculate the quantity of injected hydrogen.

$$n_{\mathrm{H}_2} = \dot{n}_{\mathrm{H}_2} \left(\Delta t_{valve} - 800\ \mu\mathrm{s}\right) \tag{12}$$

where Δt_{valve} is the duration the piezoelectric valve was programmed to stay open. Using the ideal gas expression the increase of the pressure inside the tokamak (Δp_{tok}) can also be calculated. Table V shows the results of these calculations for the discharges in study.

Table V: Calculated hydrogen injected quantities for the puffing discharges and their effects on the tokamak pressure

Δt_{valve} (ms)	n_{H_2} ($\times 10^{15}$)	Δp_{tok} ($\times 10^{-5}$ mbar)	$p_{total_{tok}}$ ($\times 10^{-4}$ mbar)
0	0	0	1.1
1.5	80.5	3.6	1.46
2	138	6.2	1.72
2.5	195.5	8.8	1.98
3	253	11.4	2.24

Considering the values on the last column of the table, it is notorious that the 2.5 ms and 3 ms puffing discharges became to close or even higher than the maximum background pressure for a stable shot which is 2×10^{-4} mbar. This increase in the tokamak pressure is too much and too quick, and the plasma instead of improving its condition gets worse.

Therefore, the system throughput should be reduced, so that less gas is injected per unit of time. This could be arranged either by reducing the inlet pressure of the piezoelectric valve or by reducing the voltage levels aplied to it (100 V).

6. CONCLUSIONS AND FUTURE WORK

The work described in this paper consisted on the development of a real-time system designed for the diagnostic of the electron plasma density based on a dsPIC30F4013. This microcontroller represents an extremely low-cost purely digital approach to the real-time calculation of the electron plasma density. Despite its limitations already discussed, the system was able to do what it was intended to in a very reliable way. The system main parameters are presented in table VI.

Table VI: Real-time system parameters

Parameter	**Value**
Maximum sampling rate	98.3 ksps
Calculation cycle	3.8 μs
Algorithm resolution	62 mrad
Maximum transmission rate	102.4 kHz
Phase range	[-5.22 $\times$ 2π, 5.22 $\times$ 2π]
Maximum electron density	2.29 $\times$ 10^{19} m^{-3}
Maximum electron density variation	2.16 $\times$ 10^{23} $\mathrm{m}^{-3}\mathrm{s}^{-1}$

Besides these characteristics, the system also has the following features:

- Automatic detection of a discharge. This way, the system can work independently not needing an external order to start the operation.
- Automatic correction of the signals and electron density offsets, increasing the precision of the calculation.
- High CPU cycle free time for other operations. Considering a sampling rate of 46.81 ksps, which produces very good results, the microcontroller is free of calculation during 82.2% of the time.
- Low latency (3.8 μs plus transmission time).
- High system versatility. This means that the system can be easily adapted to other devices than ISTTOK and that several possible configurations regarding sampling and data transmission rates can be used.

Regarding the results obtained in the several discharges performed at the ISTTOK tokamak, they were

very similar with the offline calculation, showing the quality of the system developed. However, it was seen that near the operating limits of the ADCs (very high sampling rates and low T_{AD}) the system showed an evident loss in precision.

A series of tests to the ISTTOK puffing system were also performed. This study showed that the current system has a very high throughput which can be harmful to the plasma. It should be reduced if the puffing is to be used as hydrogen fuelling in long discharges. The study of the puffing system should then be repeated in this new configuration to see the impact of the new puffing on the plasma electron density.

With the results of this last study a real-time control method for the piezoelectric valve would be developed and implemented in the real-time system described in this project. The control of the piezoelectric valve can be easily achieved with the programming of a PWM by the microcontroller. The system should be optimized to enable longer discharges at the ISTTOK tokamak.

The real-time system described can also be used in other devices with the COMPASS-D tokamak in Prague being a good candidate. This can be done right away for the real-time determination of the plasma electron density or after the real-time control of the piezoelectric valve. This change to a different device can be easily done with small adaptations in the software level to take into account the different electron density levels and interferometer.

Acknowledgments

This work has been carried out within the framework of the Contract of Association between the European Atomic Energy Community and "Instituto Superior Técnico". Financial support was also received from "Fundação para a Ciência e Tecnologia" in the frame of the Contract of Associated Laboratory.

[1] *http://www.eia.doe.gov/*. Energy Information Administration.
[2] J. Wesson. *Tokamaks*. Claarendon Press - Oxford, 2004.
[3] D. D. Ryutov. *Environmental aspects of fusion energy*. IOP Publishing Ltd, 1992.
[4] D. F. Valcárcel. Controlo em Tempo-Real da Posição da Coluna de Plasma no Tokamak ISTTOK. Master's thesis, Instituto Superior Técnico, 2008.
[5] A. A. Harms, K. F. Schoepf, G. H. Miley and D. R. Kingdon. *Principles of Fusion Energy*. World Scientific Publishing Co. Pte. Ltd, 2005.
[6] G. McCracken and P. Stott. *Fusion: The Energy of the Universe*. Elsevier Academic Press, 2005.
[7] C. A. Varandas et al. A instalação em Portugal da primeira experiência de fusão nuclear: O tokamak ISTTOK. *Gazeta de Física*, September 1991.
[8] H. Fernandes. Operação AC do Tokamak ISTTOK. PhD thesis, Instituto Superior Técnico, 1998.
[9] H. Fernandes, C. A. Varandas, J. C. Cabral, H. Figueiredo, R. Galvao and A. J. Batista. Engineering Aspects of the ISTTOK Operation in a Multicycle Alternating Flat-Top Plasma Current Regime. *Fusion Engineering, 17th IEEE/NPS Symposium*, pages 576-580, October 1997.
[10] J. C. Cabral, H. Fernandes, H. Figueiredo and C. A. Varandas. Operation of the tokamak ISTTOK in a multicycle alternating flat-top plasma current regime. *Nuclear Fusion*, 37(11):1575-1581, September 1991.
[11] D. Darling. *http://www.daviddarling.info/*. The Internet Encyclopedia of Science.
[12] F. Gardiol. *Hypérfrequences*. Dounod Press, 1987.
[13] F. Chen. *Introduction to Plasma Physics and Controlled Fusion*. Plenum Press, 1984.
[14] R. J. King. *Microwave Homodyne Systems*. Peter Peregrinus Ltd, 1978.
[15] S. Vergamota. Interferometria de micro-ondas no Tokamak IST-TOK. Master's thesis, Instituto Superior Técnico, 1993.
[16] H. R. Koslowski. A real-time multiradian phase detector for interferometry based on a digital phase locked loop circuit. *Measurement Science and Technology*, 5(3):307-309, March 1994.
[17] T. N. Carlstrom, D. R. Ahlgren and J. Crosbie. Real-time, vibration-compensated CO_2 interferometer operation on the DIII-D tokamak. *Review of Scientific Instruments*, 59(7):1063-1066, March 1988.
[18] M. Emami and H. Rasouli. Plasma electron density measurement by a digital signal processor based millimetre-wave interferometer. *Measurement Science and Technology*, 15(5):1000-1004, April 2004.
[19] T. G. Marques, A. Gouveia. T. Pereira. J. Fortunato. B. B. Carvalho. J. Sousa. C. Silva and H. Fernandes. Real-time digital heterodyne interferometer for high resolution plasma density measurements at ISTTOK. *Review of Scientific Instruments*, to be published.
[20] *http://cdaq.cfn.ist.utl.pt:8085/*. ISTTOK Control and Data Acquisition.
[21] H. Fernandes, J. Fortunato. L. Pedro and T. Pereira. Picnode board specs. 2007.
[22] *DSPIC30F Family Reference Manual*. Microchip Technology Inc., 2006.
[23] *DSPIC30F4013 Data sheet*. Microchip Technology Inc., 2006.
[24] *MPLAB C30 C Compiler User's Guide*. Microchip Technology Inc., 2007.
[25] *LM358 - Low Power Dual Operational Amplifiers Data sheet*. 2007.
[26] T. G. Marques, P. Duarte, C. Silva and H. Fernandes. Study for the real-time control of the ISTTOK hydrogen injection system. *Vacuum*, waiting referee approval.
[27] S. B. Bhatt, A. Kumar, K. P. Subramanian and P. K. Atrey. Gas puffing by molecular beam injection in Aditya tokamak. *Fusion Engineering and Design*, (75-79):655-661, July 2005.
[28] *MaxTek piezoelectric gas leak valve MV-112 manual*. Maxtek Inc.